Magnesium Technology 2011
Edited by: Wim H. Sillekens, Sean R. Agnew, Neale R. Neelameggham, and Suveen N. Mathaudhu
TMS (The Minerals, Metals & Materials Society), 2011

PRECIPITATION PROCESS IN Mg-Nd-Zn-Zr-Gd/Y ALLOY

J.H. Li[1,2*], G. Sha[2, 3], P. Schumacher[1, 4], S. P. Ringer[2, 3]

[1*] Chair of Casting Research, Department of Metallurgy, the University of Leoben, A-8700, Leoben, Austria (jiehua.li@mu-leoben.at)
[2] Australian Centre for Microscopy and Microanalysis, The University of Sydney, Madsen Building F09, Sydney, NSW 2006, Australia
[3] ARC Centre of Excellence for Design in Light Metals, The University of Sydney, NSW 2006, Australia
[4] Austrian Foundry Research Institute, Parkstrasse 21, Leoben, Styria, A-8700, Austria

Keywords: Mg-Nd-Zn-Zr-Gd/Y alloys; Age hardening; Precipitate; TEM; Atom probe tomography.

Abstract

Transmission electron microscopy (TEM) and atom probe tomography (APT) were employed to investigate the solute clusters and precipitates formed in different Mg-Nd-Zn-Zr-Gd/Y alloys aged at 200 °C up to 100 h. TEM characterizations confirmed the precipitation in these alloys involved the formation of precipitates such as β″, β′, β1 and β. Most precipitates habited on $(01\bar{1}0)_{\alpha\text{-Mg}}$ and a few thin plate (of 1-2 atomic layers in thickness) lying on $(0001)_{\alpha\text{-Mg}}$. APT analyses revealed that the precipitates were enriched with Nd, Zn and Gd. Moreover, Nd partitioned more strongly into the precipitates than Gd and Zn. In contrast, Y was less prone to partition into precipitates than other alloying elements in these alloys.

Introduction

Magnesium alloys have important applications in the automotive and aerospace industries because of their high specific strength for the weight reduction and better fuel economy [1]. However, the mechanical properties of conventional Mg alloys are often not suitable for high temperature applications. The addition of heavy rare-earth (HRE) elements, such as Nd, Gd, Y, Dy, Er, Sc, Tb and Sm etc, has been found to be effective to promote precipitation hardening and to improve the high temperature performance of Mg alloys [2-14]. Indeed, most high-strength Mg alloys such as WE54/43 and QE22 contain HRE elements. The level of alloying addition of the HRE elements is a critical concern in the alloy development and design of Mg alloys because of both material costs and the desire to have the alloy as light as possible. There is a strong interest in developing advanced Mg alloys with a low HRE addition.

The Mg-Nd-Zn based alloys [2, 3, 4], such as ZM-6 in China and ML10 in Russia, exhibit a strong age hardening response and have been used in various structural airframe components. Our previous researches [5, 6, 7] have revealed that the mechanical properties of Mg-Nd-Zn based alloy can be improved further through optimizing alloy composition and using proper heat-treatment, as well as the addition of Gd with a lower content. Specifically, an Mg-3.6Gd-2.8Nd-0.6Zn-0.4Zr (wt %, used through the paper, in case not specified otherwise) alloy has a yield strength and ultimate strength at 300 °C about 10% and 18% higher than those of an Mg-2.8Nd-0.6Zn-0.4Zr alloy, respectively. On the other hand, the addition of Y into magnesium alloys is also well-known to be one of the most effective ways to improve their mechanical properties at elevated temperatures. Mg-Y-Nd based alloys with higher Y contents, e.g. WE54 and WE43 [8], have always been regarded to be very important commercial Mg alloys. However, the addition of Y in high quantities is less attractive due to increasing alloy density and cost. Similar to the Gd addition into Mg-Nd-Zn based alloy, the only 0.2 % Y addition into Mg-2.8Nd-0.6Zn-0.4Zr based alloy has also been investigated in our previous researches [6, 7]. The Mg-2.8Nd-0.2Y-0.6Zn-0.4Zr alloy has also shown a significant improvement on tensile properties, especially the excellent tensile yield strength (TYS) at higher temperatures (200 °C -350 °C), compared with the Y-free Mg-2.8Nd-0.6Zn-0.4Zr based alloy. For example, the TYS (190 MPa) of the Y-containing alloy at room temperature is much higher than that of Y-free alloy (158 MPa) and the Gd-containing alloy with relatively higher Gd concentration 3.6 wt % (165 MPa). When tested at 200 °C, the TYS (183MPa) of the Y-containing alloy is also much higher than that of Y-free alloy (141MPa) and the Gd-containing alloy (143MPa).

The objective of this research is to characterize precipitate microstructure in order to understand their strengthening effect in these Mg-Nd-Zn-Zr-Gd/Y alloys. To date, there is a lack of information about the solute partitioning during precipitation in the alloys. In this contribution, transmission electron microscopy (TEM) and atom probe tomography (APT) were employed to characterize the solute clusters and precipitates in the Mg-Nd-Zn-Zr-Gd/Y alloys aged at 200 °C.

Experimental material and procedures

Two experimental alloys with compositions of Mg-3.6Gd-2.8Nd-0.6Zn-0.4Zr and Mg-2.8Nd-0.2Y-0.6Zn-0.4Zr were prepared with high purity Mg (99.9 %), Zn (99.9 %), Nd (99.9 %), Mg–28Gd, Mg–28Y and Mg–33Zr master alloys in an electric resistance furnace under the protection of an anti-oxidizing flux, and cast into a sand mould. The chemical compositions of the experimental alloys were determined by inductively coupled plasma atomic emission spectrum (ICP-AES) apparatus. Solution treatment were conducted at 525 °C for 18 h in a salt bath, then samples were quenched in cold water, and subsequently were aged in a oil bath at 200 °C. The Vickers hardness testing was undertaken on LECO Hardness Tester (LV700AT) with 1 kg load and 10 s dwelling time. Each data point reported in this paper represents an average of at least 10 measurements. The foil specimens for TEM were prepared by twin jet electro-polishing in a solution of 25 % $HClO_4$ and 75 % methanol at -40 °C with a voltage of 20 V and subsequently low energy beam ion thinning was used for surface cleanness. The TEM examinations were performed in a Philips CM12 operating at 120 kV and a high resolution TEM (JEOL-3000F) operating at 300 kV. The samples for atom probe analysis were prepared by micro-electro-polishing. Atom probe analyses were performed using an Imago LEAP™ 3000 operating at a specimen temperature of 20 K, 20 % pulse fraction and under ultrahigh vacuum conditions.

Results and discussions

Figure 1 shows the age hardening response for the three Mg alloys. The Gd-containing alloy and the Y-containing alloy demonstrate the higher hardening response than the base alloy. The hardness of the Gd-containing alloy increased quickly during the first 1.5 h at 200 °C and then reached plateau-like range before reaching peak hardness after 70 h. Further ageing led to over-ageing and a progressive decrease in hardness.

The age hardening response of the Y-containing alloy is higher than that of the base alloy, but lower than that of the Gd-containing alloy. This is consistent with the fact that the Y addition of 0.2 % in the Y-containing alloy is much lower than the Gd addition of 3.6 % in the Gd-containing alloy. It should be noted that the hardness of the Y-containing alloy also exhibits a strong age-hardening response during the first 1.5 h at 200 °C, with a hardness increase of 32 % from the initial hardness (58 HV) of the as-quenched sample. A similar age hardening response was also observed in other Mg alloys containing Nd [9, 10]. The significant ageing response of GN72 at 200 °C has been attributed to the rapid formation of β′, and possibly β″, precipitates during the early stages of ageing [10]. Our previous atom probe tomography data analysis [11] has indicated that the fast age-hardening response is directly correlated to the stronger partitioning of Nd in the Mg-Nd based alloy. Further ageing leads to a maximum hardness of 76 HV at about 14 h and then a progressive decrease in hardness.

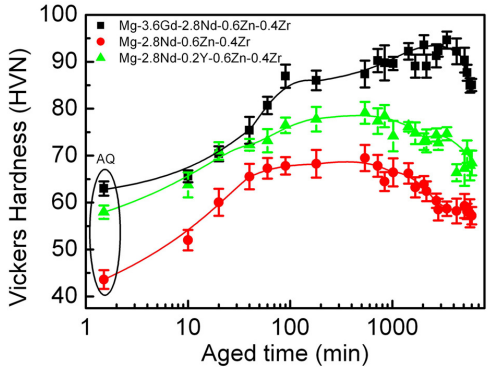

Fig. 1. Age hardening curve of Mg-2.8Nd-0.6Zn-0.4Zr (wt %) alloy aged at 200 °C. The results of the 0.2 % Y-containing and 3.6 % Gd-containing alloys are also shown.

Figure 2 is a series of representative $[01\bar{1}\,0]_{\alpha\text{-Mg}}$ bright field (BF) TEM images and the corresponding selected area diffraction patterns (SADP) of Mg-3.6Gd-2.8Nd-0.6Zn-0.4Zr alloy aged for 3 h, 14 h and 70 h at 200 °C. After ageing for 3 h, Fig. 2a reveals that the precipitates are in a high number density and are small in their sizes. The corresponding $[01\bar{1}\,0]_{\alpha\text{-Mg}}$ SADP provided in Fig. 2b indicates that the precipitates have a general habit plane or trace parallel to $\{2\bar{1}\bar{1}\,0\}_{\alpha\text{-Mg}}$ and the weak diffraction streaks at $\frac{1}{2}(2\bar{1}\bar{1}\,0)_{\alpha\text{-Mg}}$ and $\frac{1}{2}(2\bar{1}\bar{1}\,4)_{\alpha\text{-Mg}}$ (marked with a white arrow) are consistent with evidence for β″ precipitation, since this phase possesses a DO_{19} crystal structure with a hexagonal unit cell of a=b=0.64 nm and c=0.52 nm [8] and stoichiometry Mg_3X [13]. The extremely weak diffraction at $\frac{1}{2}(2\bar{1}\bar{1}\,2)_{\alpha\text{-Mg}}$, marked with a black arrow, suggests that a low number density of β′ precipitates co-exist with the more numerous β″ precipitates at this stage of ageing. The precipitate phase β′ is known to have a base-centred

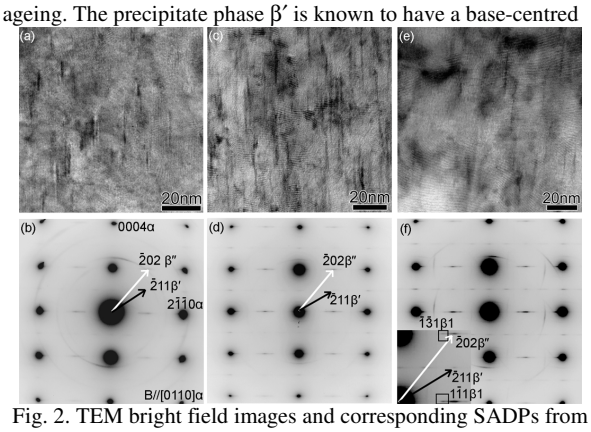

Fig. 2. TEM bright field images and corresponding SADPs from the microstructure of Mg-3.6Gd-2.8Nd-0.6Zn-0.4Zr (wt. %) alloy samples aged at 200 °C for various times: (a-b) 3 h, (c-d) 14 h and (e-f) 70 h. Incident electron beam direction is parallel to $[01\bar{1}\,0]_{\alpha}$.

orthorhombic unit cell a=0.640 nm, b=2.223 nm, c=0.521 nm [8] and stoichiometry Mg_5X [13]. After ageing for 14 h, stronger diffraction effects at $\frac{1}{2}(2\bar{1}\bar{1}\,2)_{\alpha\text{-Mg}}$ were evident in the $[01\bar{1}\,0]_{\alpha\text{-Mg}}$ SADP (marked with a black arrow in Fig. 2d), suggesting that β″ precipitates have transformed into or nucleated β′. After ageing for 70 h, a weak diffraction spot clearly adjacent to $\frac{1}{2}(2\bar{1}\bar{1}\,0)_{\alpha\text{-Mg}}$, as marked with a black box in Fig. 2f, indicates the presence of β_1 in the microstructure. The β_1 phase possesses a face-centred cubic unit cell with a=0.72 nm and stoichiometry of Mg_3X [8, 13]. The orientation relationships between the precipitates such as β", β', β_1 and the matrix are in agreement with those reported previously [8, 12, 13]. Thus, the precipitation sequence in Gd-containing alloy during ageing is supersaturated solid solution (SSSS) → β″ (DO_{19}) → β′ (bco) → β_1 (fcc).

A similar precipitation reaction was also observed in the Y-containing alloy. Fig. 3 shows a series of representative bright field (BF) TEM images and the corresponding SADP obtained from the Y-containing alloy samples after ageing at 200 °C at 14 h. After ageing at 200 °C for 14 h, the morphology of precipitates become easily distinguished in TEM images, as shown in Figs.3a and c. The $[0001]_{\alpha\text{-Mg}}$ and $[01\bar{1}\,0]_{\alpha\text{-Mg}}$ SADPs show some diffraction spots in the midway of those from the reflection of Mg matrix ($[01\bar{1}\,0]_{\alpha\text{-Mg}}$ or$[2\bar{1}\bar{1}\,0]_{\alpha\text{-Mg}}$), as shown in Figs.3b and d, respectively, suggesting that the β″ precipitates with DO_{19} structure (a=b=0.64 nm and c=0.52 nm) still existed in α-Mg matrix after ageing for 14 h, as marked with a black solid arrow in Fig. 3d. The extremely weak diffractions at $\frac{1}{2}(2\bar{1}\bar{1}\,1)_{\alpha\text{-Mg}}$ in $[01\bar{1}\,0]_{\alpha\text{-Mg}}$ SADP, as marked with a white solid arrow in Fig. 3d, suggest that β′ precipitates co-existed with β″ precipitates at this stage of ageing. The precipitate phase β′ was also known to have a base-centred orthorhombic unit cell a = 0.640 nm, b = 2.223 nm, c= 0.521 nm [8], and has a lamella-like morphology with a longitudinal axis parallel to $[0001]_{\alpha\text{-Mg}}$. In contrast to the Fig. 2d, there is no clear diffraction spot adjacent to $\frac{1}{2}(2\bar{1}\bar{1}\,0)_{\alpha\text{-Mg}}$ in $[01\bar{1}\,0]_{\alpha\text{-Mg}}$ SADP, as marked with a white box in Fig. 3d. However, the HRTEM images and corresponding fast Fourier transform (FFT), as shown in Figs. 4b and c, indicates that the β_1 precipitate does exist in the microstructure. It should be noted that

the FFT analysis was obtained from the areas only containing β_1 precipitate. As shown in Fig. 4a, the β_1 precipitates seam to be isolated.

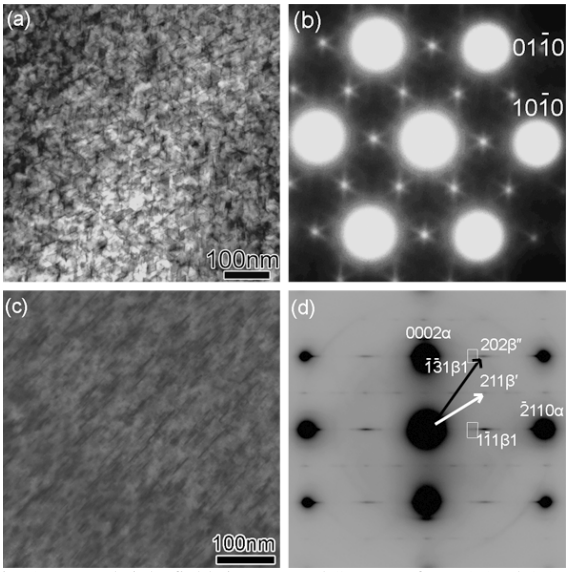

Fig. 3. TEM (bright field) images and SADPs of Mg-2.8Nd-0.2Y-0.6Zn-0.4Zr (wt %) alloy aged at 200 °C for 14 h. (a), (b) Incident electron beam direction is parallel to $[0001]_{\alpha\text{-Mg}}$; (c), (d) Incident electron beam direction is parallel to $[01\bar{1}0]_{\alpha\text{-Mg}}$.

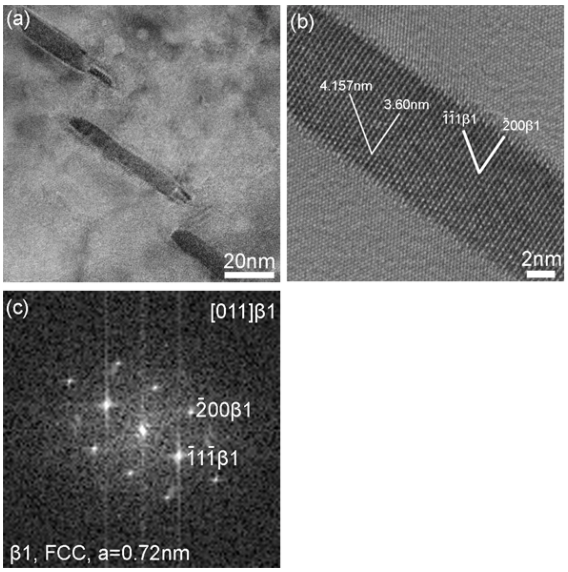

Fig. 4. Low magnification (a), high magnification (b) HRTEM image and FFT (c) of the precipitates in Mg-2.8Nd-0.2Y-0.6Zn-0.4Zr (wt %) alloy aged at 200 °C for 14 h. Incident electron beam direction is parallel to $[0001]_{\alpha\text{-Mg}}$.

No β′ precipitates are associated with them at all. This is different from the report in [8, 12, 13] in which the β_1 phase is suggested to form via an invariant plane strain transformation of the magnesium lattice, with the specific morphology of the rhombic shape connecting with the β′ phase. The β′ phase present in contact with the smaller facets of the β_1 plates were suggested to be a consequence of shear strain accommodation. As suggested in [10], the nucleation of the β_1 phase may be independent of β′ globules, although the β_1 phase is also connecting with β′ phase in all of the alloys investigated in [10]. The formation of the β_1 precipitate may be correlated to a solute-rich region between the two β′ phases caused by the nucleation of β′ phases (Mg_5X) on the existing β″ plates along the length of β″ phase (Mg_3X). This solute-rich region provides an idea nucleation sites for the β_1 phase. The alloying elements partitioning into the precipitates can be further confirmed with our atom probe analysis.

The equilibrium β phase was not observed in both the Y-containing alloy and the Gd-containing alloy after ageing at 200 °C for 14 h and 70 h, respectively. We suppose that the equilibrium β phase, which possess a face-centred cubic unit cell with a=2.223 nm and stoichiometry of Mg_3X [8] eventually precipitates in this system, though it was not observed over the time-scale of our ageing experiments at 200 °C. Thus, the precipitation sequence in the Gd-containing alloy during ageing is, supersaturated solid solution (SSSS) → β″ ($D0_{19}$) → β′ (bco) → β_1 (fcc)→ β (fcc). We propose that the β″ precipitates are primarily responsible for the age hardening effects at 200 °C observed in Fig.1 up to around 3 h ageing whereafter the effect of β′ precipitates predominates.

Viewed from $[11\bar{2}0]_{\alpha\text{-Mg}}$, a few thin precipitates on the basal plane are also observed in Y-containing alloy after aged at 200 °C up to 14 h. As marked with white solid arrow in Figs. 5a and b, these precipitates are only about 2 atomic layers in thicknesses in Y-containing alloy. For clarity, the β series precipitates are also marked with a white box in Figs. 5a and b. With increasing ageing time, the length increases from about 10 nm (3 h) to about 20 nm (14 h), but the thickness does not change greatly. The very thin precipitates on the basal plane have been observed in [14] and designated as the γ series precipitates. The further investigations about the γ series precipitates in this alloy system are in progress.

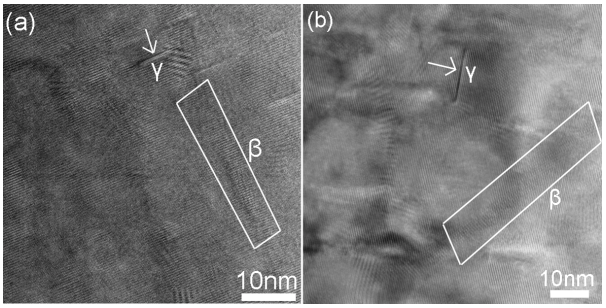

Fig. 5. HRTEM images of Mg-2.8Nd-0.2Y-0.6Zn-0.4Zr (wt %) alloy aged at 200 °C for 3 h and 14 h, respectively. (a) 3 h; (b) 14 h, Incident electron beam direction is parallel to $[11\bar{2}0]_{\alpha\text{-Mg}}$.

Some very thin precipitates on the basal plane are also observed in Gd-containing alloy after aged at 200 °C for 14 h, as shown in Figs. 6d, e and f. The γ precipitates are perpendicular to the β precipitates, and are rich in Nd, Gd and Zn. Figs. 6 a, b and c also provides a series of three-dimensional atom maps recorded from our atom probe experiments on specimens of the Mg-3.6Gd-2.8Nd-0.6Zn-0.4Zr alloy after ageing at 200 °C for (a) 3 h (b) 14 h and (c) 70 h. It is clear that all three of the main solute elements, Nd, Gd and Zn are directly imaged within the precipitates. By examining the precipitates from different directions, it is also clear that most precipitates are elongated with their longitudinal axis parallel to $[0001]_{\alpha\text{-Mg}}$ and this is in agreement with previous TEM

observations for β″, β′ and β_1. From the $[0001]_{\alpha\text{-Mg}}$ view direction, it is clear that the precipitate size increases with ageing time. It is also noteworthy that the number density of precipitates appears to

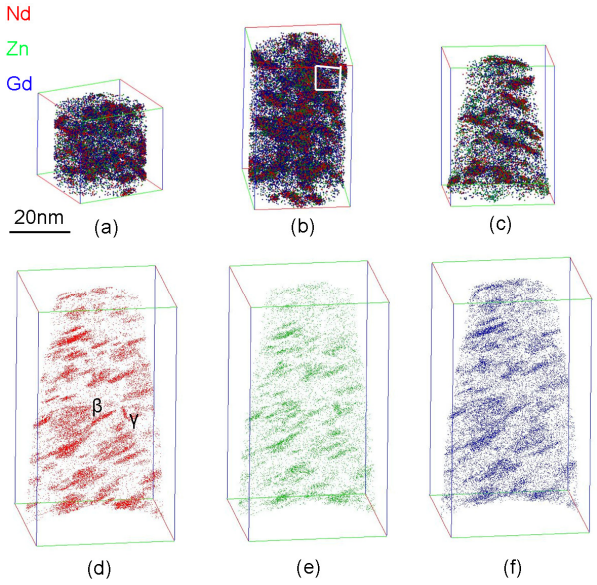

Fig. 6. Combined atom maps of Nd (red), Gd (blue) and Zn (green) obtained from Mg-3.6Gd-2.8Nd-0.6Zn-0.4Zr alloy samples aged at 200 °C for (a) 3 h, (b)14 h and (c) 70 h, in a view direction close to the $[0001]_{\alpha\text{-Mg}}$ zone axis, and (d), (e) and (f) are high resolution atom maps of a small region in the 14 h sample (marked with white box in Fig.6(b)).

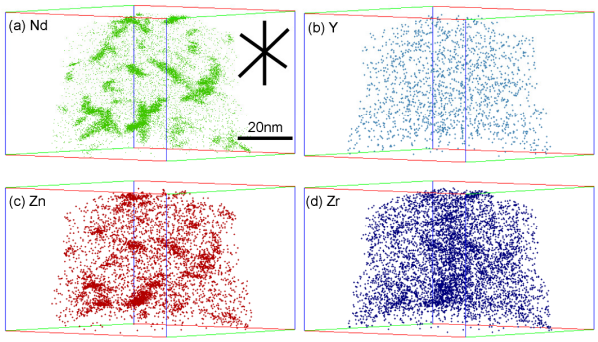

Fig. 7. APT elemental maps obtained from Mg-2.8Nd-0.2Y-0.6Zn-0.4Zr (wt %) alloy aged at 200 °C for 14 h. (a) Nd (green); (b) Y (blue); (c) Zn (red); (d) Zr (purple)

be highest in the sample aged 3 h and that this progressively decreases when compared to the precipitate number density after ageing for 14 and 70 h. In fact, our analysis of total number density (not shown here) reveals that there are less precipitates by a factor of 10 in the material aged 70 h at 200 °C compared to the material aged 3 h and yet the hardness is 10% higher in the 70 h material. Consistent with other reports [8, 13], this suggests that the β′ and β_1 are more potent hardening obstacles than the β″ phase.

In contrast, the Y solute element shows less prone to partition into precipitates than other alloying elements in Y-containing alloy. After ageing at 200 °C for 14 h, the Y solute element is still distributed in the α-Mg matrix, rather than partition into these precipitates, as shown in Fig. 7, although the distribution of solute elements in precipitates, including Nd, Zn, Zr and Y, is more uniform than that after ageing 3 h (not shown here). From these APT element maps, especially the element maps of Nd shown in Fig. 7a, it can be easily found that the length of the precipitates is about 20nm (14 h). This is consistent with our previous TEM observation (Fig. 3). More importantly, the distribution of the precipitates is nearly along three different directions, as marked with black solid line in Fig. 7a. This is also consistent with our previous TEM observation viewed from $[0001]_{\alpha\text{-Mg}}$ (Fig. 3a).

Conclusions

The precipitation microstructure evolution and the precipitation sequence in the Mg-Nd-Zn-Zr-Gd/Y alloys involve in the formation of phase as β″, β′, β_1 and the γ precipitates. These precipitates are enriched with Nd, Zn and Gd. Y appears to be less prone to partition into precipitates than any other alloying element in these alloys. A combined addition of Gd and Y into Mg-Nd-Zn alloy can be expected to be a promising way to further improve the age hardening response.

Acknowledgements

The authors are grateful for scientific and technical input and support from the Australian Microscopy & Microanalysis Research Facility (AMMRF) node at the University of Sydney. Jiehua Li also wishes to thank the China Scholarship Council for the financial support to his study in the University of Sydney.

References

[1] B.L.Mordike, *"Creep-resistant Magnesium Alloys,"* Mater. Sci. Eng. A ., 324 (1-2) (2002), 103-112.

[2] T.J. Pike, B Noble, *"The Formation and Structure of Precipitates in a Dilute Magnesium-Neodymium Alloy,"* J. Less Common Metals., 30 (1) (1973), 63-74.

[3] P.A. Nuttall, T.J. Pike, and B Noble, *"Metallography of dilute Mg-Nd-Zn alloys,"* Metallography., 13 (1980), 3-20.

[4] L.R. Gill, G.W. Lorimer, P. Lyon, *"The Effect of Zinc and Gadolinium on the Precipitation Sequence and Quench Sensitivity of Four Mg-Nd-Gd alloys,"* Adv. Eng. Mater., 9 (9) (2007), 784.

[5] J.H. Li, W.Q. Jie, G.Y. Yang, *"Effect of Gadolinium on the Aging Hardening Behavior, Solidification Microstructure and Mechanical Properties of Mg-Nd-Zn-Zr Cast Magnesium Alloys,"* Trans. Nonferrous Met. Soc. China., 18 (2008), s27-32.

[6] J.H. Li, W.Q. Jie, G.Y. Yang, *"Effect of Gadolinium on Microstructures and Mechanical Properties of Mg -Nd-Zn-Zr Cast Magnesium Alloys,"* Rare Metal Materials and Engineering, 37 (2008), 1751-1755.

[7] J.H. Li, W.Q. Jie, G.Y. Yang, *"Influences of Alloying Element Zn on the Microstructure and Mechanical Properties of GW series Magnesium Alloys,"* Acta Metallurgica Sinca. 10 (43) (2007), 1077-1081.

[8] J.F. Nie, and B.C. Muddle, *"Characterisation of Strengthening Precipitate Phases in a Mg–Y–Nd Alloy",* Acta Mater., 48 (8) (2000), 1691-1703.

[9] K.Y. Zheng, et al., *"Precipitation and its Effect on the Mechanical Properties of a cast Mg–Gd–Nd–Zr Alloy,"*

Mater. Sci. Eng. A., 489 (1-2) (2008), 44-54.
[10] P.J. Apps, et al., *"Precipitation Reactions in Magnesium-Rare Earth Alloys Containing Yttrium, Gadolinium or Dysprosium,"* Scripta Mater., 48 (8) (2003), 1023-1028.
[11] G Sha, et al., "Atom Probe Tomography Characterization of Early-stage Precipitates in an Mg-Gd-Nd-Zn Alloy," *8th International Conference on Magnesium Alloys and Their Application.*, ed. K.U. Kainer, (Wiley-VCH, 2009), 40-45.
[12] T Honma, et al., *"Chemistry of Nanoscale Precipitates in Mg–2.1Gd–0.6Y–0.2Zr (at.%) Alloy Investigated by the Atom Probe Technique,"* Mater. Sci. Eng. A. 395 (1-2) (2005), 301-306.
[13] T Honma, et al., *"Effect of Zn Additions on the Age-Hardening of Mg–2.0Gd–1.2Y–0.2Zr Alloys,"* Acta Mater., 55 (12) (2007), 4137-4150.
[14] J.F. Nie et al., *"Solute Segregation and Precipitation in a Creep-resistant Mg–Gd–Zn Alloy,"* Acta Mater., 56 (20) (2008), 6061-6076.